Analysis of Vasculature for Liver Surgical Planning

Dirk Selle, Bernhard Preim*, Andrea Schenk, and Heinz-Otto Peitgen

Invited Review

***Abstract*—For liver surgical planning, the structure and morphology of the hepatic vessels and their relationship to tumors are of major interest. To achieve a fast and robust assistance with optimal quantitative and visual information, we present methods for a geometrical and structural analysis of vessel systems. Starting from the raw image data a sequence of image processing steps has to be carried out until a three-dimensional representation of the relevant anatomic and pathologic structures is generated. Based on computed tomography (CT) scans, the following steps are performed. 1) The volume data is preprocessed and the vessels are segmented. 2) The skeleton of the vessels is determined and transformed into a graph enabling a geometrical and structural shape analysis. Using this information the different intrahepatic vessel systems are identified automatically. 3) Based on the structural analysis of the branches of the portal vein, their vascular territories are approximated with different methods. These methods are compared and validated anatomically by means of corrosion casts of human livers. 4) Vessels are visualized with graphics primitives fitted to the skeleton to provide smooth visualizations without aliasing artifacts. The image analysis techniques have been evaluated in the clinical environment and have been used in more than 170 cases so far to plan interventions and transplantations.**

***Index Terms*—Feature extraction, image segmentation, liver surgery, vessel visualization.**

I. Introduction

AN ACCURATE analysis of vascular systems in volumetric image data is gaining increasing importance for a variety of medical applications. Precise knowledge of the morphology and structure of a vascular system allows for quantitative diagnosis, surgical planning, and outcome assessment, as well as for monitoring of the progression of vascular disease [47].

A. Planning in Liver Surgery

In this paper, we focus on computational methods for the analysis and visualization of hepatic vascular structures for liver surgery planning. One of the most challenging problems in liver surgery is to assess the morphology and branching pattern of the hepatic vasculature and their supply volume. The large variety of these branching patterns is illustrated in textbooks on anatomy (see, for example, [31]).

Manuscript received July 15, 2001; revised February 26, 2002. The Associate Editor responsible for coordinating the review of this paper and recommending its publication was M. W. Vannier. *Asterisk indicates corresponding author.*

D. Selle, A. Schenk, and H.-O. Peitgen are with MeVis–Center for Medical Diagnostic Systems and Visualization, University of Bremen, D-28359 Bremen, Germany.

*B. Preim is with MeVis–Center for Medical Diagnostic Systems and Visualization, University of Bremen, Universitätsallee 29, D-28359 Bremen, Germany (e-mail: preim@mevis.de).

Digital Object Identifier 10.1109/TMI.2002.801166

The development of the methods presented here is motivated and guided by the following two clinical applications.

1) Living-related liver transplants (LRLT): These operations are required by the lack of organs needed for transplantation. LRLT is a procedure where a healthy voluntary donor gives a part of his or her liver to another person. These transplantations are feasible due to the regenerative power of the liver. A careful analysis of the branching pattern and morphology of all hepatic vessel systems is a precondition for LRLT. Additionally, volumetric approximations are carried out to predict the postoperative liver function. With this analysis, the decision whether a person is suitable as a donor for LRLT is supported.
2) Oncologic resections: For patients with liver cancer or liver metastasis, e.g., from colorectal cancer, resectability is an essential question. Resectability and the extent of the required resection depend primarily on the location of tumors and the spatial relations between tumors and major hepatic vessels.

For the planning of both these operations, it is crucial to provide the surgeon with a patient-individual three-dimensional (3-D) representation of the liver along with its vasculature and lesions. Such a representation allows for an exploration of the vascular anatomy and the measurement of vessel diameters and distances, as well as the analysis of the shape and volume of vascular territories. All of this is based on an accurate segmentation and analysis of the intrahepatic vessels.

B. Overview

In this paper, we present new methods to analyze the patient's intrahepatic vasculature from clinical computed tomography (CT) volume data. As a result, a 3-D model of the relevant structures is generated which enables more precise access to the individual intrahepatic vasculature and builds a new basis for preoperative planning. To achieve this, we will discuss the following four steps.

1) *Vessel segmentation*: The intrahepatic vessels are segmented with a refined region-growing algorithm to meet the demands of runtime, robustness, and level of automation for acceptance in clinical routine.
2) *Analysis of vessel structures*: Algorithms based on graph theoretical methods are used to analyze the geometry and the ramification structure of the segmented vessels. For this purpose, the skeletons of vessels are determined.
3) *Model-based approximation of vascular territories*: The territories that are supplied by the main branches of the portal vein are determined. We present evidence for the

Fig. 1. 2-D slice of a CT volume dataset. The applied contrast agent provides a high vessel-to-tissue contrast and reveals the highlighted portal vein and some branches of the hepatic vein. The two dark spots inside the liver represent liver metastasis. (Dataset provided by Prof. Galanski, Medical School Hannover.)

accuracy of these methods based on studies of corrosion casts of eight human livers.

4) *Vessel visualization*: Based on the skeletons and the information concerning the vessel diameter, antialiased vessel visualizations are generated by fitting graphics primitives along the skeleton lines.

Finally, an interactive 3-D visualization is provided which allows the user to explore the previously identified and analyzed structures. The following sections describe these steps.

II. Medical Background

Because of the complex vascular anatomy of the liver, surgical interventions are challenging. Four different vessel systems supply and drain the liver: the portal vein, hepatic vein, hepatic artery, and bilary ducts. A successful operation requires enough remaining liver tissue supplied by all four vessel systems. Since the portal vein, the hepatic artery, and the bile ducts parallel, the portal vein is regarded as the leading structure for these three vessel systems.

For a surgeon, it is difficult to mentally construct the 3-D structure of vessel systems based on planar slices of radiological data (cf. Fig. 1) and to estimate which part of a vessel system would be damaged as a consequence of a surgical intervention [22]. In order to enable surgeons to perform liver resections respecting the vascular anatomy, a schematic model of the liver was introduced by Couinaud [4]. Following this model, the human liver can be divided into different *segments* which are determined according to the branching structure of the portal vein. A liver segment is defined by the supplied territory of a third-order branch of the portal vein. Since these segments are independent from each other, they can be resected without damaging the supply of the other segments. Applying the widespread scheme of Couinaud directly is questionable from an anatomical point of view, since the liver segments are highly variable in shape, size, and number (see Fasel *et al.* [11]). Therefore, it is desirable to identify the individual liver segments preoperatively.

III. Methods

A. Fast and Robust Vessel Segmentation

The segmentation of the intrahepatic vessels is a prerequisite for a subsequent geometrical and structural analysis. In a preprocessing step, filter functions for noise reduction (Gaussian, median filter) and for background compensation (Laplace-like filters) are applied to the CT data [42]. For background compensation, the size of the filter kernel is chosen such that it is larger than the thickest vessel inside the liver (default is 15×15). The application of this filter is restricted to an interval which is defined such that the lower interval bound roughly corresponds to the gray value of the liver parenchyma and the upper bound corresponds to the brightest values inside the liver.

As a result, intrahepatic vessels can be identified and delineated by using a threshold-based region-growing method. Usually, region-growing segmentation must be repeated with modified thresholds until an appropriate result is found. To accelerate this procedure, we refined the procedure to automatically suggest a threshold.

Initially, a seed voxel of the portal vein close to its entrance into the liver is selected interactively. Starting with this seed voxel, the region-oriented segmentation algorithm iteratively accumulates the 26 adjacent voxels with an intensity equal to or greater than the intensity θ_{beg} of the seed voxel and keeps them in a list $L(\theta_{\mathrm{beg}})$. Using $L(\theta_{\mathrm{beg}})$ as new seed voxels, all adjacent voxels with intensities greater than or equal to $\theta_{\mathrm{beg}} - 1$ are collected in a list $L(\theta_{\mathrm{beg}} - 1)$. The threshold is further decreased until a given threshold θ_{end} is reached which definitively creates only voxels $L(\theta_{\mathrm{end}})$ outside the vessel systems.

The generation of the voxel lists is performed efficiently because voxel lists for the segmentation with threshold $\theta - 1$ have already been constructed when using the threshold θ. In total, some 100 lists are generated which takes approximately 3–5 s on modern PC hardware for high-resolution CT datasets (512×512 matrix with slice distance 3 mm).

The automatic threshold selection is based on the observation that the number of voxels $N(\theta)$ is approximately linear decreasing for $\theta = \theta_{\mathrm{opt}} \cdots \theta_{\mathrm{beg}}$ (Fig. 2). At θ_{opt}, the slope changes considerably because many voxels belonging to the liver tissue are collected for thresholds below θ_{opt}. Thus, a suggestion for θ_{opt} can be found by calculating an optimal fit of two straight lines for $N(\theta)$. For this purpose, the two characteristic parts of the curve are approximated by two regression lines. The points $(\theta_{\mathrm{beg}}, |N(\theta_{\mathrm{beg}})|) \cdots (j, |N(j)|)$, respectively, $(j+1, |N(j+1)|) \cdots (\theta_{\mathrm{end}}, |N(\theta_{\mathrm{end}})|)$ are employed to calculate the correlation coefficients for both lines. j is chosen such that the sum of the two correlation coefficients is maximal.

We found that the position of the crossing of both regression lines yields a good suggestion for θ_{opt} in most cases. If the suggested threshold is not satisfying, it may be changed interactively. On the basis of the generated voxel lists $L(\theta_{\mathrm{beg}}) \cdots L(\theta_{\mathrm{end}})$, the vessel system specified by any threshold θ can be displayed very fast by simply drawing all precalculated voxels from the lists $L(\theta_{\mathrm{beg}}) \cdots L(\theta)$.

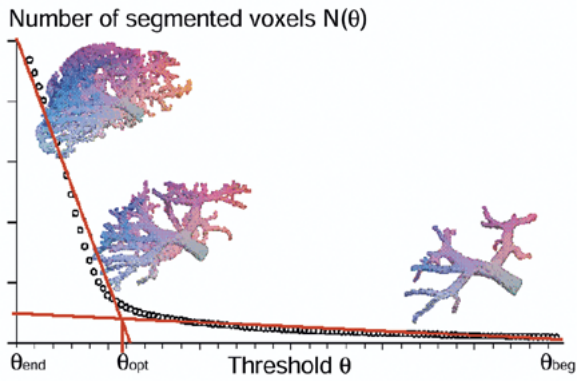

Fig. 2. Estimation of an optimal threshold for vessel segmentation. (©Springer 2000, originally published in [43], reprinted with permission.)

B. Graph-Based Analysis of Vasculature

The segmentation result is a set of voxels representing the intrahepatic vessel systems. For surgery planning, a further analysis of these voxels is required. This includes geometric measurements of the branches (radius, length) and the identification of the ramification pattern (e.g., to determine the main portal subtrees supplying the liver segments).

Before the analysis of the vessel systems is carried out, a segmentation problem due to imaging artifacts has to be approached. Depending on the scanning protocol, usually two or more different vessel systems of the liver are enhanced with contrast agent during the scan. Often the portal and hepatic vein are affected, which are shown in Fig. 3(a). Therefore, the scan yields high-intensity voxels for both vessel systems. Due to the limited spatial resolution of the scanned volume data, voxels of different vessel systems are often adjacent to each other such that they are segmented as one object when in reality there is only proximity between the two. A manual separation of the different vessel systems would be too time consuming for clinical routine. Therefore, we analyze and separate such "forests" of connected vessel systems automatically using graph theoretical methods. In a first step, the voxel-based shape representation of the vessels is transformed into an abstract graph representation, utilizing "skeletonization." The skeleton representation carries all information about the original shape of the object and, at the same time, facilitates an algorithmic geometrical and structural shape analysis. The principal approach is illustrated in Fig. 4.

1) Skeletonization: The skeleton, or medial axis in two dimensions (2-D), of an object in continuous 2-D space is defined as the set of all points which are equidistant from at least two points on the boundary of the object [3]. In discrete space, this definition cannot be applied directly. Since the discretization generally produces jagged surfaces, many irrelevant skeleton branches would arise. We use "thinning" as a basic technique for the skeletonization and, thus, successively erode the surface voxels of an object, until the skeleton remains. During this process, three aspects are crucial to preserve the properties of continuous skeletons and to yield skeletons which reflect the original shape of the vessel system.

1) The erosion of the voxels must not change the topology of the original structure, i.e., the number of connected objects, cavities, and 3-D holes must remain the same.

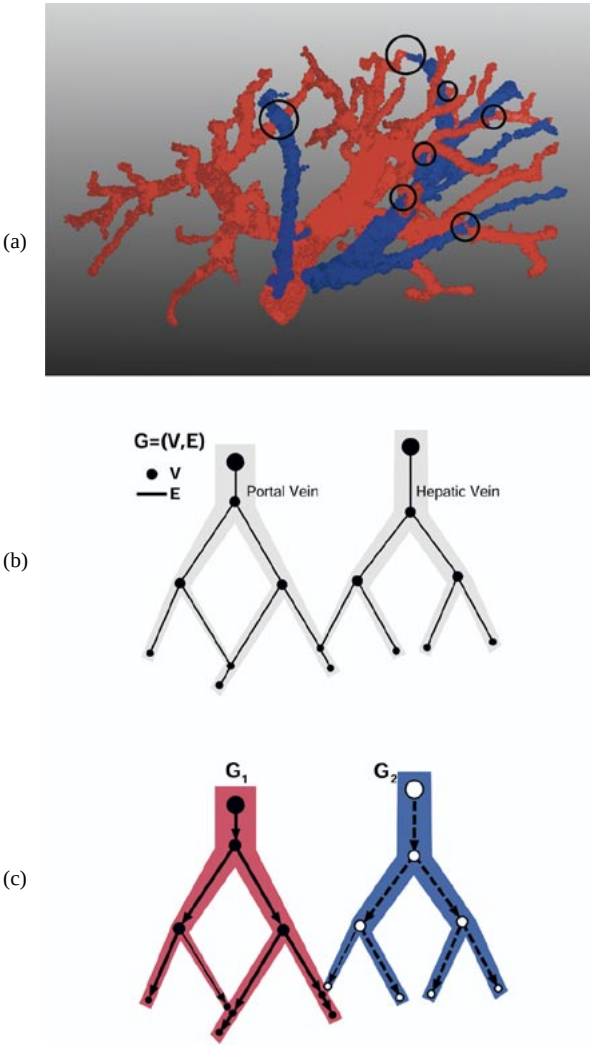

Fig. 3. (a) Portal vein (red) and fragments of the hepatic vein (blue) as result of the vessel segmentation based on an underlying CT examination, in which both vessel systems are enhanced with contrast agent. Both systems touch at the encircled points of contact and cannot be segmented separately. (b) Graph G of two touching vessel systems. (c) Orientation of G, which consists of directed acyclic graphs G_1 and G_2. (©Springer 2000, originally published in [43], reprinted with permission.)

2) The erosion must be carried out symmetrically to provide a reliable and accurate central position of the skeleton.
3) Noisy vessel surfaces should not lead to "irrelevant" skeleton lines, which would be mistakenly interpreted as side branches.

Although many 2-D skeletonization algorithms have been developed for applications ranging from optical character recognition to biological cell studies (see, e.g., [21] for a survey), relatively few methods exist for the 3-D case (see Section V-D).

In our skeletonization approach, it is checked for each voxel whether its deletion preserves the 3-D topology of the object. Voxels with this feature are called *simple points* [19] and only these are deleted in the erosion process. Efficient methods to detect simple points are described, e.g., by Davies and Lee [6], [23].

To cope with anisotropic voxels, special care of a precise symmetric erosion was required. Therefore, we combined the skeletonization with a distance transformation and introduced a

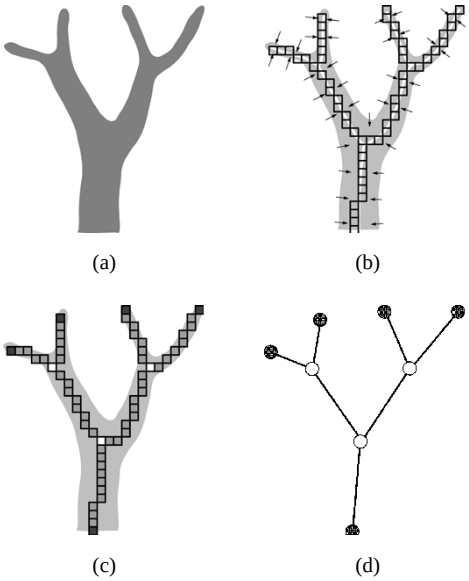

Fig. 4. Transformation of (a) voxel-based shape representation of vessels into a graph is performed in three steps: (b) skeletonization using thinning techniques; (c) identification of voxels, which represent ramifications or endpoints of the vessel system, and (d) creation of a corresponding graph for a further analysis. (©Springer 2000 originally published in [43], reprinted with permission.)

three-component distance label [5] which is propagated during the thinning process. In each thinning step, only those voxels with the same Euclidean distance to the boundary of the object are eroded [42].

To deal with the varying quality of the medical datasets, we control the creation of "irrelevant" skeleton lines which usually appear due to noise. Fig. 5 illustrates a vessel tree with several side branches at the right boundary. To distinguish "relevant" and "irrelevant" side branches, we consider the gradient of the distance transformation [Fig. 5(c)]. The main branches of the tree create "mountain ridges" in the distances to the boundary which have a steepest gradient close to zero. Side branches also create ridges, but their steepest gradient θ is larger than zero and smaller than one. For all other points, θ is close to one. Based on a threshold decision on the steepest gradient θ, we define irrelevant side branches. In Fig. 5(b), for example, all skeleton endpoints with $\theta - 0.6$ were not eroded during the thinning process. This yields skeleton lines for all of the side branches which are, thus, considered to be "relevant" structural information. In Fig. 5(c), only skeleton endpoints with $\theta = 0$ were preserved from erosion. Fig. 6 shows the skeleton of the segmented vessel systems from a clinical dataset with different values for θ. It turned out that for clinical data, $\theta = 0$ is most appropriate [Fig. 5(c)] to identify vascular structures and to avoid irrelevant branches. This threshold means that only voxels with a local maximum in the distance transform belong to the medial axis. We fixed θ for clinical applications in hospitals. The skeletons which are used for vascular analysis (see the following sections) also use this value.

2) Graph Analysis: Compared with the voxel-based shape representation of the segmented vessels, the skeleton representation enables a much easier access to the geometry of the branches (medial axis and radius) and to structural information (ramifications). For further analysis, the skeleton is interpreted

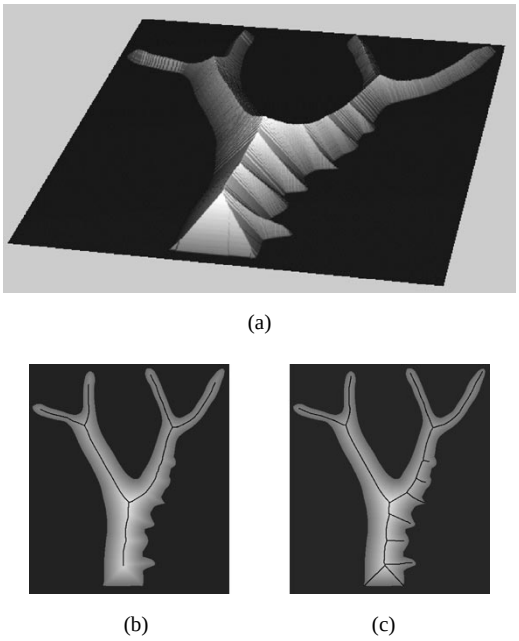

Fig. 5. (a) Distance transformation of the segmented vessel tree illustrated as a 3-D visualization where the ridges represent the center line. The steepest gradient can be used as indication for the relevance of a side branch. (b) Skeleton of a vessel tree with some side branches at the right boundary. The side branches are interpreted as structural information and are represented by a skeleton line. For each point of the tree, the distance from the boundary is coded in a corresponding gray value. (c) In this case, the side branches are interpreted as noise which are, therefore, not represented by skeleton lines. (©SPIE 2001, originally published in [44], reprinted with permission.)

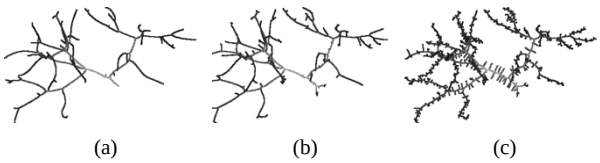

Fig. 6. Skeleton of the segmented vessels. For the skeletonization, a threshold of (a) 0, (b) 0.8, and (c) 0.9 was chosen for the steepest gradient of the distance transform. Depending on the threshold, more or fewer skeleton lines appear. Most of the skeleton lines in (c) are due to noise. (© SPIE 2001, originally published in [44], reprinted with permission.)

as a graph $G = (V, E)$, whose vertices V represent ramification points and whose edges E represent the parts between the ramifications. The average radius of the corresponding branch is assigned to each edge.

Based on this graph representation, the problem of separating different vessel systems can be described and solved as follows. Given a graph representation G of the connected portal and hepatic veins, we have to determine an orientation of G that consists of directed acyclic graphs G_i with the following properties: The root of each directed graph G_i corresponds to the root of the portal tree, to the root of the hepatic veins, or to the roots of accessory or fragmental subtrees of the hepatic veins [as in Figs. 3 and 7(a)]. All directed paths in G_i lead from the root to the periphery of the corresponding vessel system.

To determine the trees G_i, first, the root R of one of the vessel systems is automatically chosen as root for G_0. A reasonable candidate for the root can be found at the edge with maximal radius. At this edge, the vertex most distant from the center of gravity of the vessel systems is chosen. As an alternative, the root can be set interactively. Starting with $G_0 = (\{R\}, \{\})$, for

all adjacent vertices of G_0 the connecting edge with the maximal radius is added as a forward edge to G_0. This procedure is repeated iteratively, also considering the new adjacent vertices of G_0. The definition of new roots of trees or subtrees depends on a user-defined parameter $n = 1 \cdots \infty$. If there exists an edge in G that is not already added to G_0 and that has a radius which is more than n times greater than the maximal radius of the adjacent edges of G_0, a new root candidate is determined and set as initial vertex in G_1. The process of adding adjacent edges to G_0, G_1, ... is continued until all edges of G have been considered. The resulting directed graphs G_i have the following properties.

- Each path in G from the root of G_i to G_j is separated at the edge with minimal radius.
- Each cycle within G_i is resolved at the edge with minimal radius.
- Following a directed path in G_i from the root to the periphery, a once reached branch radius can increase only n-fold. If n is chosen sufficiently large, only one graph G_0 is created. For $n = 1$, the radius of each created tree G_i never increases along the paths from root to periphery, which typically yields a large number of separated trees G_i for clinical data. The choice of n determines the sensitivity of the separation into subtrees. Best results have been obtained with $n = 0.5$, although in a few cases, this value had to increased or decreased slightly.

If the automatic vessel separation does not succeed completely, interaction facilities can be used to manually set the root of a vessel system or to identify touching points. Using the described algorithm for the skeleton shown in Fig. 7(a), the portal tree (white) and two fragmental subtrees of the hepatic vein (blue) were detected. Besides this, the graph representation of the vessels is also the basis for user interactions such as defining the hierarchical structure of trees, subtrees, and paths. Furthermore, it allows to measure the radius, length, or volume of branches. In Fig. 7(b), the hepatic vein was removed automatically using the above described methods. The main branches of the portal vein were identified automatically by determining the eight most voluminous portal subtrees, which are assumed to supply the various liver segments. The identification of these branches is a prerequisite for the approximation of the patient's individual liver segments [Fig. 7(c)], described in the next section.

C. Model-Based Approximation of Liver Segments

For liver surgery, the knowledge of the shape and volume of the patient's individual liver segments is essential to estimate the risk of different resection strategies. Due to the limited spatial resolution, only the major branches of the portal vein can be extracted. Referring to the liver, the problem can be described as follows. Assume that L is the set of all voxels in the medical volume data V representing the liver. Let $B \subset L$ denote the set of voxels belonging to the extracted portal tree. B is the union of the main branches or subtrees $B_i \subset B$, $i = 1, \ldots, n$, which supply the portal segments (Section III-A and -B for the determination of B and B_i).

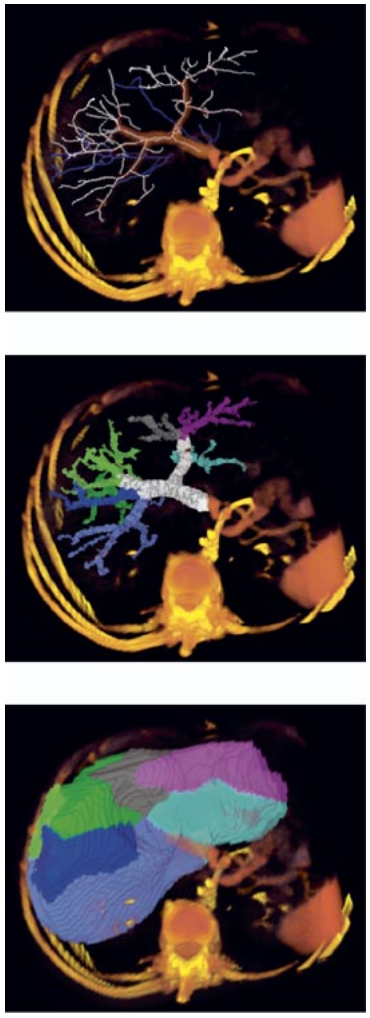

Fig. 7. (a) Skeleton of the extracted vessels from the dataset shown in Fig. 1. The hepatic veins (blue) are separated from the portal vein automatically. (b) Automatic determination of the main branches of the portal vein. (c) Liver segments supplied by the portal vein branches in (b). (©Springer 2000, originally published in [43], reprinted with permission.)

To determine the liver segments, we have to find a function g: $L \rightarrow \{1, \ldots, n\}$, which assigns to each liver voxel $v \in L$ a segment number i, provided v is supplied by the branch B_i. The set of all voxels supplied by this branch represents the liver segment i and is denoted by S_i. To compensate the missing information about the portal tree and to predict the segmental anatomy, we suggest model-based approaches to determine g, which consider the patient's individual anatomy represented by given L and B_i.

The definition of a realistic function must reflect the probability that the sprouts of the various incomplete subtrees B_i reach and supply a liver voxel v. Measures for this "reachability" [illustrated by arrows $d_1, \ldots, d_4$ in Fig. 8(b)] can be expressed by a metric. A voxel v then is assigned to that branch B_i which has the shortest distance with respect to a suitable metric. The choice of a metric is difficult since the blood supply is realized by complex branching structures, whose formation process is not fully understood (see [16] for a discussion). For this reason, we describe and evaluate two approaches using two different metrics: the nearest neighbor segment approximation

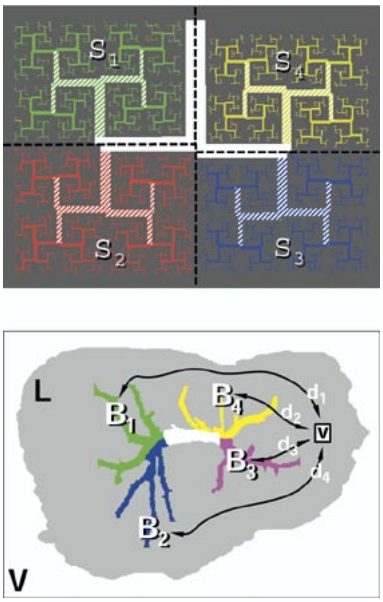

Fig. 8. Problem of the segment approximation. (a) Ideal situation: The detailed and dense branching structure of the mathematically constructed tree directly indicates the supported territories s_i of the four hatched main branches. (b) Clinical situation: Only the main portal branches b_i can be extracted, which do not directly reveal the liver segments. (©Springer 2000, originally published in [43], reprinted with permission.)

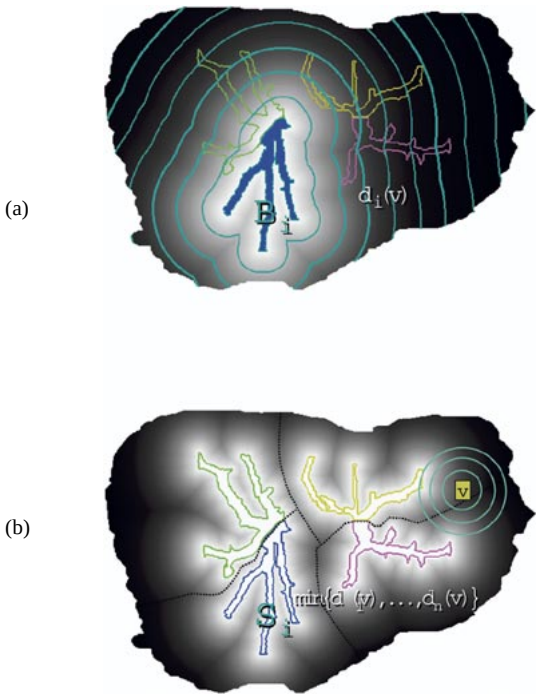

Fig. 9. NNSA using the Euclidean metric. (a) Euclidean distance $d_i(v)$ for the branch B_i: the darker a liver voxel, the greater is the distance $d_i(v)$ to the branch B_i. The indicated lines are equidistant from B_i. (b) The minimum of the distance functions for all branches reveals the segment boundaries (see the dotted lines). (©Springer 2000, originally published in [43], reprinted with permission.)

(NNSA), introduced in Section III-C-2, and the Laplacian segment approximation (LASA), which exploits a metric derived by potential functions in Section III-C-3. The use of potential functions was inspired by recent advances in statistical physics dealing with growth models for branching structures known as Laplacian fractals (lightning, viscous fingering, electrochemical deposits, and other deposits driven by diffusion) [1], [8], [9]. The LASA method is based on a fundamental equation of physics and offers interesting venues for a scientific understanding of the prediction method. The NNSA method is conceptually simple and has rather low computational complexity.

1) Liver Segmentation: To extract the liver L, we developed semiautomatic segmentation tools (based on live-wire techniques [10], [30], [49]). With live-wire segmentation, the user starts with selecting a first contour point and moves a pointing device (for example, a mouse) to roughly sketch the object's contour. The algorithm relies on a cost function to calculate an optimal path between the start point and the current position of the pointing device in real time. The cost function is a weighted sum which considers the magnitude and direction of the gradient and the Laplacian zero crossing. With this approach, a few user-defined contour points lead to a piecewise optimal user-steered segmentation. The initial approach has been carefully refined in order to enhance 3-D segmentation. For this purpose, live-wire is combined with shape-based interpolation [38] between interactively segmented contours and subsequent optimization. This new approach computes the majority of the contours automatically and, therefore, reduces the interaction effort. The required time can be shortened by some 70% (depending on the slice distance, up to 85% for high-resolution multislice CT data) [40], [41].

2) NNSA: For each branch B_i ($i = 1, \ldots, n$), we define the Euclidean distance

$$d_i(v) = \min_{v' \in B_i} \|v - v'\|_2 \qquad \text{where } v \in L. \tag{1}$$

Using this metric, liver voxels $v \in L$ are assigned to the branches as follows:

$$g_{\mathrm{NNSA}}(v) = k \quad \text{where } d_k(v) = \min\{d_1(v), \ldots, d_n(v)\}. \tag{2}$$

Finally, the set of all liver voxels assigned to b_i is defined as liver segment S_i

$$S_i = \{v \in L | g_{\mathrm{NNSA}}(v) = i\}. \tag{3}$$

In other words, $d_i(v)$ is the Euclidean distance of the voxel v to the nearest voxel belonging to B_i [see Fig. 9(a)]. According to this metric, the closer a liver voxel v is to a branch B_i, the more likely it is for v to be supplied by B_i.

The function g_{NNSA} assigns to each liver voxel v the nearest branch B_k [cf. Fig. 9(b)]. This figure also shows the minimal distance $\min\{d_1(v), \ldots, d_n(v)\}$ for each liver voxel v. The result of the NNSA method is shown in Fig. 7(c), which is based on the portal branches in Fig. 7(b).

3) LASA: The Laplacian method defines for each branch B_i ($i = 1, \ldots, n$) the potential function $\phi_i(v)$, which solves the Laplacian equation

$$\nabla^2 \phi_i(v) = 0 \qquad \text{when } v \in L \tag{4}$$

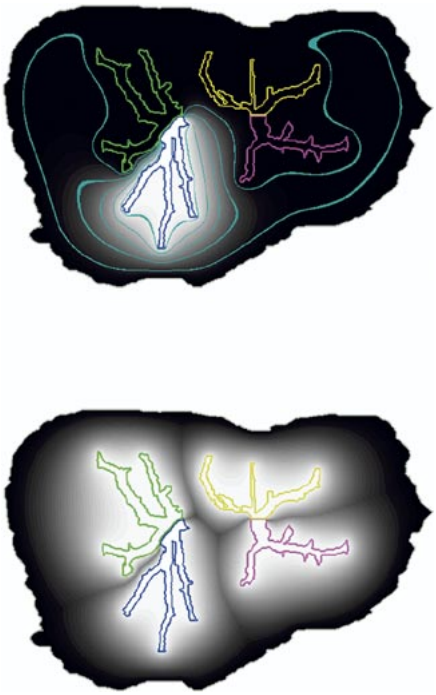

Fig. 10. LASA using a metric based on potentials. (a) Potential ϕ_i for the branch B_i: The potential is set to 1 (white) for all voxels belonging to B_i and to 0 (black) for the other branches and the region outside the liver. The gray values for the other voxels indicate the potential ranging between 0 and 1. The lines indicate surfaces of equal potential. (b) The maximum of the potential functions for all branches reveals the segment boundaries. (©Springer 2000, originally published in [43], reprinted with permission.)

and satisfies the boundary conditions

$$\phi_i(v) = 1 \qquad \text{when } v \in B_i \tag{5}$$

$$\phi_i(v) = 0 \qquad \text{when } v \in B_j,\ j \neq i \tag{6}$$

$$\phi_i(v) = 0 \qquad \text{when } v \notin L. \tag{7}$$

The liver voxels $v \in L$ are assigned to the branches as follows:

$$g_{\mathrm{LASA}}(v) = k \qquad \text{where } \phi_k(v) = \max\{\phi_1(v), \ldots, \phi_n(v)\}. \tag{8}$$

The liver segments are defined as

$$S_i = \{v \in L \,|\, g_{\mathrm{LASA}}(v) = i\}. \tag{9}$$

The potential $\phi_i(v)$ for one of the branches is illustrated in Fig. 10(a). Contrary to the Euclidean distance $d_i(v)$, the potential $\phi_i(v)$ depends for each voxel v on *every* detail of the completely known anatomy B and L.

The function g_{LASA} assigns each liver voxel v to that branch B_k which contributes the largest potential $\phi_k(v)$ to v. This assignment is indicated in Fig. 10(b), which is a rendering of the maximal potential for each liver voxel v. The local minima of the potential, which again appear as "dark valleys," separate the territories dominated and supplied by the different branches B_i. The result of this method is shown in Fig. 11(b). Even though the LASA and NNSA method differ strongly in their formulation and computational complexity, they yield rather similar results [Fig. 11(c)].

4) Extension of the LASA: Since the Laplacian equation describes different fundamental laws in physics, the LASA

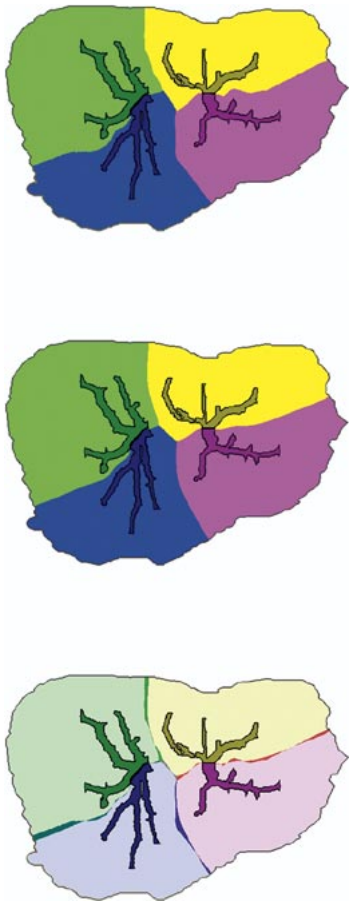

Fig. 11. Results of the segment approximation methods: (a) NNSA. (b) LASA. (c) Difference of both methods. The voxels, which are assigned to different segments are enhanced with dark colors. (©Springer 2000, originally published in [43], reprinted with permission.)

method of liver segments can be interpreted in several different ways. One way is to think of a diffusion process. The branches B_i keep up a constant concentration of blood, which diffuses into the liver. According to this assumption, the segment S_i then is that part of the liver to which the branch B_i contributes the highest concentration of blood, thus, having the highest probability of being supplied by B_i. This interpretation is speculative and needs to be validated. But contrary to the NNSA method, this model of blood supply can be extended in quite a natural way. Since the hepatic vein drains the blood out of the liver, one can introduce an additional boundary condition

$$\phi_i(v) = 0 \qquad \text{when } v \in \text{hepatic vein} \tag{10}$$

which defines the hepatic vein as a sink for blood particles.

Furthermore, it seems reasonable that the amount of blood which is delivered by a portal branch depends on the size of the branch. Instead of using the boundary condition in (5), which assumes a constant potential 1 for all branches B_i, we introduce a modified boundary condition

$$\phi_i(v) = r(v) \qquad \text{where } v \in B_i \tag{11}$$

and where $r(v)$ is the local radius of the branches at the position v. Using this boundary condition, the influence of smaller branches is reduced in comparison to the larger branches.

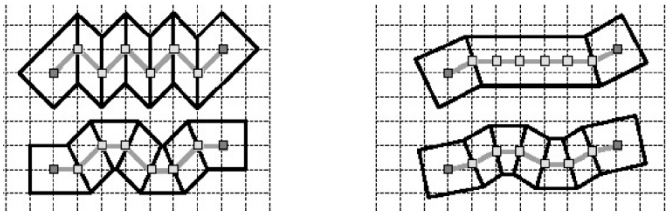

Fig. 12. Smoothing with a binomial filter. The jagged skeleton on the left is transformed into the smoother skeleton on the right. Small quadrilaterals represent the voxel centers. Note that the start and end points of the skeleton are unaffected.

Using these boundary conditions, which incorporate additional anatomical information, the reliability and accuracy of the LASA method of the liver segments can be improved.

5) Implementation: The calculation of liver segments with the NNSA method relies on a distance transformation which is also employed for the skeletonization (Section III-B-1). This algorithm properly handles anisotropic voxels (thus, a transformation to isotropic voxels is not required).

For the solution of the Laplace equation, relaxation methods are used which are described in [36]. For this purpose, the potential is regarded as a diffusion process with a time variable t. Starting with an initial distribution and the current boundary conditions, the diffusion is iteratively calculated until it converges. The error bound used as a criterion for convergence determines the runtime of this procedure. The approach is accelerated with multigrid techniques; however, it still takes considerable time with typical clinical data sets (e.g., $512 \times 512 \times 60$ voxels). With the error bound 0.001, it took approximately 30 min to determine the liver segments on a typical workstation. With this error bound, 98.2% of the voxels are assigned to the same segments compared to an error bound of 0.0001, which is assumed to produce the correct LASA result.

D. Visualization of Vasculature

The information derived in the skeletonization and graph analysis (Section III-B-1 and III-B-2) can be used for a high-quality vessel visualization. High quality here refers to the ability of a visualization to highlight structural information, in particular, the branching pattern of vasculature. Our method for vessel visualization is based on the assumptions that vascular systems are connected structures and they may be represented by a circular cross section.

The basis for the visualization of vasculature is the skeleton together with the information concerning the vessel diameter. The edges of the resulting skeleton are smoothed with a one-dimensional binomial filter with length 3 resulting in continuous skeleton lines (see Fig. 12). For all voxels of the skeleton with two neighbors, e.g., in the absence of branchings, the skeleton is strongly improved. However, at branchings the simple smoothing may cause undesirable effects. For example, in the case of a small bifurcation, the main branch is pulled toward the small bifurcation. Therefore, the smoothing process was modified at branchings in such a way that the voxels involved are weighted as to their relevance. As a measure for the relevance of voxel v, the size of the subtree which is dependent on the corresponding node V in the bifurcation graph G is employed. Precisely, the total length of all subbranches of node V is used to assess the relevance of v.

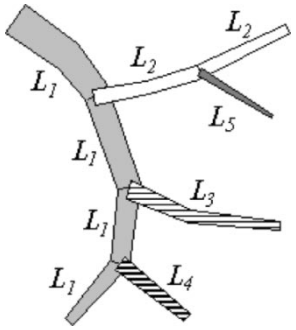

Fig. 13. Sequential edges of the vascular tree are mapped to different lists as prerequisite for the visualization via extrusions. Edges with the same gray value belong to the same list.

Due to the limited spatial resolution of CT scanners, the vessel diameter derived from the skeletonization varies often, in particular, for small vessels. If the vessel diameter is directly used for the visualization, annoying artifacts would occur. To eliminate these aliasing artifacts, the strategy which has been developed to smooth the skeleton path is reused. A binomial filter is employed to smooth the vessel diameter along the skeleton path. Again, emphasis is put upon avoiding new artifacts arising at branchings by considering the relevance of all voxels which coincide. As smoothing operations may, in principle, remove important information, the user can disable smoothing.

For the visualization of vascular structures, an extension of OpenGL, the GLExtrusions, is used. With this library, graphics primitives with a certain shape may be extruded along a path. For the visualization of vascular structures, a vascular tree is mapped to a set of lists L_i which comprise sequential edges of a vascular tree. The edges of each list represent the path used for the extrusion. As the interpolation of surface normals is applied to the edges of one path, it is desirable to assign as many edges as possible to one list. If two possible paths have the same number of edges, the path with the longest total length is chosen. The mapping of a vascular tree to the lists L_i starts at the root of the tree and searches the longest path to a leaf node. All edges involved are assigned L_1. This strategy is applied recursively to each subtree until all edges belong to a list. Fig. 13 illustrates the process for a simple 2-D tree. For each list, concatenated graphics primitives are fitted to the path. It turns out that truncated cones are able to represent the constriction of the vessel diameter appropriately. Finally, concatenated truncated cones are visualized by means of the GLExtrusions library. We refer to this method as high-quality vessel visualization (HQVV).The HQVV method and the interaction techniques for exploring vasculature are described in detail by Hahn *et al.* [17].

It must be noted that this visualization method is not suitable for virtual endoscopy because vertices inside the tubular structures are created at branchings, which would be annoying when a virtual camera is moved inside.

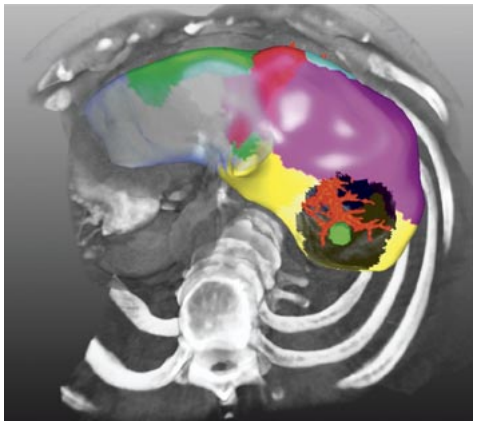

Fig. 14. Selective resection tool is used to interactively attempt the resection. The vessels are not affected by the virtual resection. Thus, it becomes obvious which parts of the vessel system are involved in the planned resection.

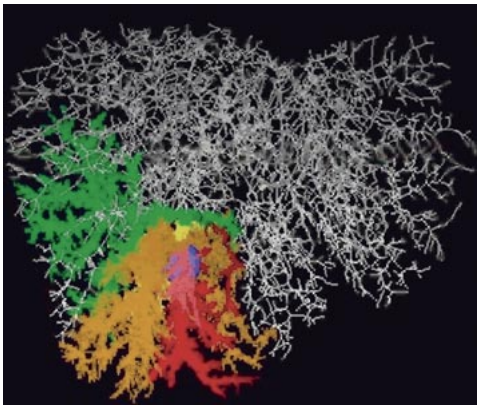

Fig. 15. Sphere as a model for a tumor has been placed in the 3-D model of a corrosion cast. Different colors indicate which parts of the portal venous system are affected in the resection of the tumor with different margins (0.5 cm: red; 1.0 cm: orange; 1.5 cm: yellow; 2 cm: green). (©Springer 2000, originally published in [43], reprinted with permission.)

E. 3-D Visualization and Surgery Planning

After image processing and analysis steps are carried out, all objects which have been identified and determined by approximation are integrated in a 3-D visualization. Here, the user can choose arbitrary viewing directions and has the flexibility of 3-D interaction. The user can assign arbitrary colors and transparency values and, thus, design individual visualizations. Furthermore, annotations which provide information, for example, about the volume of a structure, can be displayed.

Over and above a flexible 3-D-visualization, the user can preoperatively try resection strategies to pre-estimate the consequences of a surgical intervention. For this purpose, two approaches have been developed: interactive specification of resection areas and automatic proposals of how to resect lesions.

For the interactive resection, several tools have been developed which might be scaled and moved within the data [35]. Resection tools can be applied selectively such that only certain structures are affected (see Fig. 14).

The traditional method of segment-oriented surgery planning is to determine the localization of a tumor in one or more liver segments and resect them entirely. However, this approach may lead to unnecessarily large resection volumes and suffers from the problems of determining individual liver segments precisely. As an alternative approach, resection areas are suggested based on an analysis of the desired safety margin around a tumor. Based on the tumor localization and the desired margin, all affected vessels are identified. The methods described in Section III-C are used to estimate the area which is supplied by these vessels (see Fig. 15). As a consequence, the determined volume should be removed together with the selected tumor. With this approach, the surgeon concentrates on the tumor and may easily try different safety margins, where the consequences (the devascularized territories) are computed, highlighted, and quantitatively analyzed.

The strategies for resection proposals have been applied to CT data of several corrosion casts as well as to some clinical data [34]. In most of the cases, the extent and shape of the resection volumes correspond well to clinical practice. In cases where a tumor is located on the central dorsal part of the liver, the "suggested" resection volume is not accessible *in situ*.

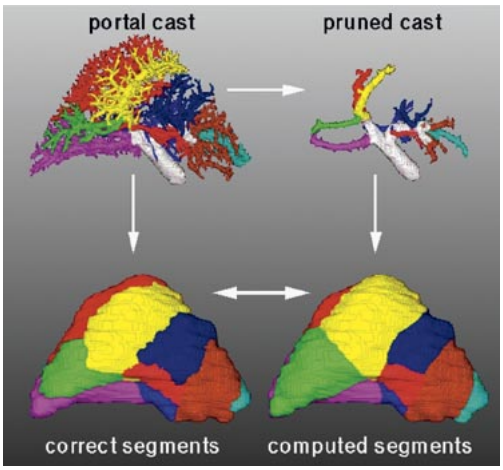

Fig. 16. Scheme of the validation of the approximation methods. (©Springer 2000, originally published in [43], reprinted with permission.)

IV. Validation and Evaluation

A. Anatomical Validation With Corrosion Casts

The validation of the methods for segment approximation is based on a study on vascular corrosion casts of the human liver. The portal and hepatic veins of unembalmed cadavers were injected *in situ* with resin. After hardening of the injected liquid, the liver was removed from the body and corroded, which leaves the detailed branching structure of the vessel systems.

High-resolution CT scans (slice distance 1 mm) of the eight casts allow us to extract the portal branches with an accumulated length of about 10–18 m (contrary to *in vivo* data with a length of only 1–1.5 m). This yields sufficient branching generations and allows us to determine very accurately the location and geometry of the portal segments of the liver.

For this work, we chose the branches B_i defining the segments according to the widespread scheme of Couinaud (Fig. 16, upper left). The gaps between the branches were closed with morphological dilation and erosion operations. Due to the large number of branching generations extracted, the resulting solid portal segments S_i provide a very precise approximation of the true anatomical segments. The derived

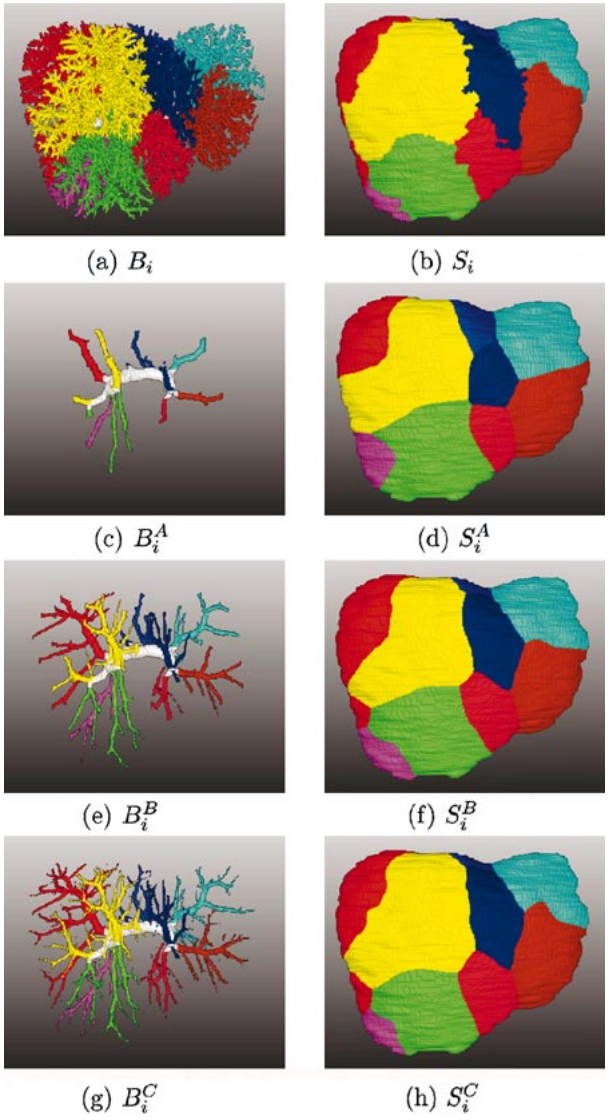

Fig. 17. Rendering of the portal vein obtained from a CT scan of a human liver cast. The main subtrees in (a) are assigned different colors revealing the liver segments. The pruned vessels in (c), (e), and (g) simulate the rather incomplete trees obtained from *in vivo* CT scans. Based on these pruning levels, the liver segments in (d), (f), and (h) are predicted with the LASA method and compared with the authentic anatomical segments in (b). (©Springer 2000, originally published in [43], reprinted with permission.)

segments have been compared with liver segments manually specified by anatomists (Fasel *et al.* [11]). To simulate the incomplete portal trees obtained from *in vivo* radiological data, we systematically pruned the trees obtained from the casts (Fig. 16, upper right). Finally, the predictions made for the pruned casts (Fig. 16, lower right) and the exact segment anatomy of the cast (Fig. 16, lower left) were compared to validate the approximation methods.

For the validation study, we distinguish three degrees of pruning, covering the different "quality levels" of the portal vein, which are expected to be found in clinical CT data:

B_i^A: the main branches of the Couinaud subtrees B_i [Fig. 17(a)]. These were determined by a radiologist, and are sometimes referred to in the literature as third-order branches.

TABLE I
RESULTS OF THE LASA AND NNSA METHODS. VOLUME OVERLAP: MEAN (STD) FOR EIGHT CASTS

Pruning level	A	B	C
NNSA	79.0% (3.6)	89.9% (2.9)	93.4% (2.9)
LASA	77.7% (3.5)	88.6% (2.6)	91.7% (2.9)
Ext. LASA	81.7% (3.5)	90.8% (2.8)	92.7% (2.9)

B_i^B: one more generation of branches than in B_i^A [Fig. 17(b)].

B_i^C: one more generation of branches than in B_i^B (Fig. 17).

B. Results

The resulting vascular trees are shown for one of the casts in Fig. 17(c), (e), and (g). The approximated segments based on these trees are denoted by S_i^A, S_i^B, and S_i^C. Results for the LASA method (without extended boundary conditions) are shown in Fig. 17(d), (f), and (h), and can be compared with the authentic anatomical segments S_i [Fig. 17(b)] based on the unpruned subtrees B_i [Fig. 17(a)].

A quantitative evaluation of the accuracy of the approximation methods was carried out in different ways: the volumetric overlap between the approximated and the authentic segments as well as the distance between the approximated segment borders and the correct segment borders have been determined [42]. Here, we focus on the volumetric overlap computation. For each cast, for each pruning level $L = A, B, C$ and for each segment $i = 1, \ldots, n$, we computed the volume $V(S_i \cap S_i^L)$ of the overlap between the authentic segment S_i and the approximated segment S_i^L. Thus, we obtained the percentage amount of correctly classified voxels $\sum_{i=1}^{n} V(S_i \cap S_i^L)/V(L) * 100\%$ for the whole liver, where $V(L)$ is the liver volume.

The results of the approximations naturally improve with the level of detail available for the portal tree (see Table I). The standard deviations specified in the Table refer to all segments of a cast. Larger values have found for each individual segment (in particular, for smaller segments). The amount of ramifications in portal trees extracted from clinical CT data lies between the pruning levels A and C. Therefore, we expect for clinical data that the NNSA method will predict the portal segment volumes with an accuracy between 80% to 90%.

The effect of incorporating the hepatic vein using the boundary condition in (10) (Section III-C-4) is illustrated in Fig. 18. Comparing Fig. 18(a) and (b), the segmental boundaries are obviously attracted by the hepatic vein (gray spots) in Fig. 18(b). Since anatomical examinations have shown that the hepatic vein typically proceeds between the liver segments [this property is confirmed in Fig. 18(c)], the accuracy of the LASA method is improved locally when considering the hepatic vein. In this case, for example, the local volumetric overlap of the blue segment is improved by 10%. We refer to the LASA method which considers the hepatic vein as extended LASA. The improvement which could be achieved with the extended LASA method is summarized in the last row of Table I. It turns out that for pruning level A, the effect is most noticeable, resulting in an approximation superior to the NNSA method. For

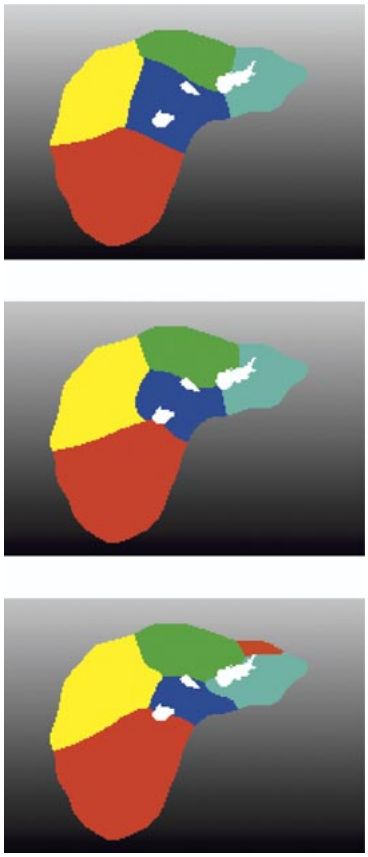

Fig. 18. Effect of the LASA method with consideration of the hepatic vein. This example shows a 2-D slice of one of the casts with the additional hepatic vein drawn in gray and colored liver segments. The segments in (a) are based on the LASA method using the pruned portal tree only, in (b) on the LASA method with additional consideration of the hepatic vein, and in (c) on the unpruned portal tree revealing the authentic liver segments. (©Springer 2000, originally published in [43], reprinted with permission.)

pruning level C, even the extended LASA method is slightly less correct compared with the NNSA method. Considering the local radius of the branches using the boundary condition in (11), we found that the results of the LASA method become more robust against reconstruction artifacts of the portal tree. The supplied territory of a thick portal branch, for example, is much less affected if some of its thinner side branches are cut off. This situation may appear in clinical data, due to pathological changes of the vessel structure, which impede the flow of the contrast agent.

C. Clinical Evaluation

In addition to the anatomical validation, our methods have been evaluated in the clinical environment for more than 170 cases to date (Medical School Hannover, University Hospital Essen, and the hospitals in Hof and Krefeld). For the planning of liver resections in patients with liver tumors, the liver, tumors, arteries, portal vein, and hepatic vein were extracted from CT data and visualized in 3-D with our software assistant HepaVision. It has been shown that these visualizations allow a suitable interactive planning of liver resections and improve the preparation especially of complex liver resections [18]. The intraoperative findings agree with the 3-D visualizations.

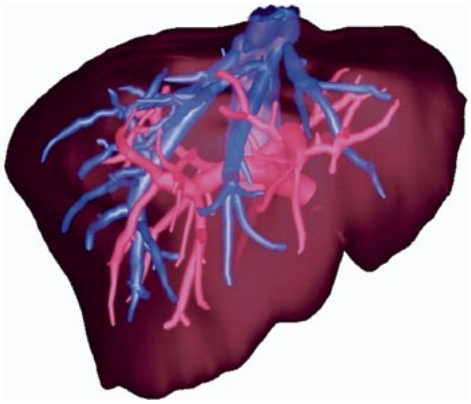

Fig. 19. HQVV of the intrahepatic vascular anatomy (hepatic vein and portal vein). The vessel diameter is smoothed.

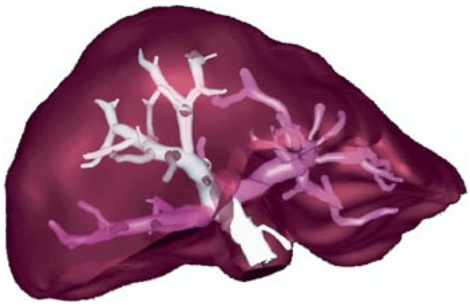

Fig. 20. Patient evaluated as a potential donor for a living transplant. The HQVV method reveals a trifurcation, a unusual anatomic variant. Because of this variant, an operation was considered to be too risky.

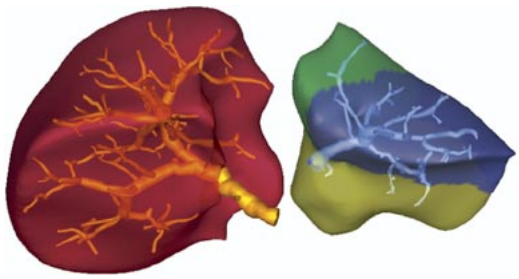

Fig. 21. Preoperative planning of split-liver resections: The liver can be split by separating three segments from the rest of the liver. The HQVV method is used to display the portal vein.

Especially for LRLT, surgeons at the Medical School Hannover regularly use the 3-D reconstruction and volumetric analysis which are carried out by radiologists using our system [12]. The vascular anatomy is crucial in the evaluation of potential donors. There are many different variants of the primary branching pattern of each of the vascular systems [31]. The next three images relate to applications in LRLT planning. As a first example, the vascular anatomy of a potential donor's liver is shown (Fig. 19). Two colors are employed to highlight the portal vein and the hepatic vein. Fig. 20 depicts an anatomic abnormality of a portal venous system, and Fig. 21 shows the separation of graft and remaining donor liver. The vessel visualization methods, which have originally been developed to visualize vessel trees from corrosion casts, have turned out to be useful for surgery planning.

For the acceptance in a clinical setting, the time required to carry out the image analysis is crucial. Using the feedback provided by the clinical partners, HepaVision has been improved significantly over the last four years and migrated from Silicon Graphics Hardware to Windows-based PCs. In this process, the graphical user interface, the facilities to generate visualizations and animation sequences, have been enhanced. With the current version, preoperative planning takes an experienced user an hour on average for oncologic cases and 45 min for planning of LRLT where tumor segmentation and risk analysis are not relevant. The following times give an idea how the total time is spread over individual steps: import DICOM data and select a region of interest (5 min), liver segmentation (10–15 min), tumor segmentation (5 min), preprocessing, vascular segmentation and skeletonization (5 min), vascular analysis (10–15 min), risk analysis (10–15 min), generation of snapshots and animation sequences (5–10 min). Risk analysis has been introduced recently and can be further improved.

V. Related Work

The crucial aspect of the work presented in this paper is the integration of all aspects of vessel analysis for clinical use. Robustness, efficiency, and interactive controllability are essential. We begin this section with a short discussion of related work on liver surgery planning and then discuss methods to efficiently and reliably solve individual tasks of vessel analysis.

A. Liver Surgical Planning

Only a few groups worldwide deal with image analysis for liver surgery planning. A group in France has developed robust methods for the analysis of clinical data for liver surgery planning [45]. Liver segmentation as well as the segmentation of intrahepatic structures are carried out fully automatically [46]. The underlying idea for the automatic liver segmentation is to start with the segmentation of more prominent surrounding structures (skin, bone, lung, kidney), thereby restricting the search space for the liver location. The intensities of the parenchyma, lesions, and intrahepatic vasculature are estimated by fitting a Gaussian to the image histogram. The separation of vascular systems is based on different geometrical considerations. First, branches which create loops in the skeleton are removed. The enhanced skeleton is then analyzed with respect to angles at branchings. Vascular structures are separated in one of two topological cases, namely, if tangency or crossing of different vascular structures are encountered and if angles at these branches are above a threshold.

The methods have been applied to 30 clinical cases. According to the literature, the methods work reliably in the majority of the cases for a precise imaging protocol of high-resolution spiral CT data. The drawback of the automatic approach, however, is a lack of interactive controllability if the assumptions are not fulfilled. A group at the German Cancer Research Institute Heidelberg developed a system for liver surgery planning [14], [15] and evaluated its use [22]. Both groups also approximate Couinaud liver segments using the NNSA method (Section III-C-2).

B. Vessel Segmentation

A variety of methods for the 3-D segmentation of vasculature, in particular, from intracranial [2], retinal [55], pulmonary, and abdominal volume data (see [47] for an overview) has been developed. Region-growing methods similar to our approach (Section III-A) are widely used; however, they differ considerably in their applicability to clinical images due to data preprocessing and the degree of interactive controllability. For example, in [51], the assumption that some 5% of the volume data are occupied by vasculature is employed. An appropriate portion of the histogram is selected and the corresponding voxels are used as input for the region-growing. Dokladal *et al.* [7] describe a modified region-growing algorithm which considers topological properties of vasculature for the extraction of liver blood vessels. Multiscale methods for vessel segmentation, which exploit local and global features of vessels for segmentation, have been proposed by Lorenz *et al.* [26] and Martinez-Perez *et al.* [28].

An alternative approach to explicit vessel segmentation is axis detection where vessel segmentation and skeletonization are integrated (see Section V-D).

C. Skeletonization and Graph Analysis

Recently, 3-D skeletonization algorithms have been developed as part of a vessel analysis pipeline or in order to compute a path for virtual endoscopy. For virtual endoscopy, a skeleton without branchings and without loops is required.

For the analysis of vasculature, Masutani *et al.* [29] developed an algorithm based on mathematical morphology. The algorithm controls irrelevant side branches of skeletons utilizing structure elements of different sizes. The segmentation method of Sonka [48] is part of a pipeline for vessel analysis. The tree structure of vessels is derived by a dilatation along the axis. Structural features are extracted to separate intracranial vessel systems (arteries and veins).

For vessel segmentation and vessel analysis, the concept of fuzzy connectedness has also been employed. This theory was originally applied to magnetic resonance (MR) brain segmentation and lesion detection [50] and later modified for analysis of vascular structures by Lei, Rice, and Udupa [24], [39]. Local fuzzy affinity (spatial nearness and region homogeneity) was combined with a global measure for fuzzy connectedness to perform vessel segmentation and the separation of different vascular systems. A more recent paper describes the methods and their clinical application in detail [25].

D. Combination of Vessel Segmentation and Skeletonization

Methods to obtain a vessel axis from 3-D images have been reviewed by Wink [52]. These are subdivided into *direct* and *indirect* approaches, where direct approaches track the vessel axis in the original data without prior vessel segmentation. Indirect approaches, on the other hand, often have difficulties with large variations in the size of the objects tracked (for example, in the vicinity of a stenosis). An example for a direct skeletonization approach is given in [32] where confocal images are analyzed.

Wink *et al.* [51], [52] present a direct approach for medial axis determination which considers the high variations of vessel shape and size in CT and MR angiographies (MRAs). The method relies on the manual determination of two points which define a first segment of the central axis. In each iteration, the vessel axis is extended by one point (the candidate point) and a plane, which is perpendicular to the current segment is constructed. A center likelihood measure is defined to evaluate points in the plane and to detect the center of the vessel (the point with the maximum center likelihood). Based on the new center point, the next candidate point is determined by extrapolation along the current medial axis.

The skeletonization method by Yim *et al.* [53] is particularly suited for small vessels in MRAs. It is based on an ordered region-growing (ORG) where an image is represented as an acyclic graph which may be reduced to a skeleton by specifying desired vessels end points and by pruning small branches. The ORG algorithm constructs a graph which represents the connectivity of all voxels based on intensity information. The drawback of this method is that all leaves of the vessel tree have to be specified, which is not necessary with the methods described in this paper. Irrelevant branches are avoided by a threshold criterion on their length. This criterion, however, is less appropriate than the suppression of skeleton branches (Section III-B-1). Yim *et al.* [54] developed a direct approach to vessel skeletonization as a basis for the detection and quantification of stenosis from MRA data. They employ a deformable model which allows for high variability in the vessel cross section and for high curvature of vessels.

E. Reconstruction of Vessels for Visualization

The benefits of the reconstruction of vascular structures enabling a visualization which emphasizes the connectivity and shape features was recognized early [13]. Vessels have been displayed with tubes after the extraction of topological filters [29]. A smooth transition of the tubes at branching points, however, is not considered. Methods for the visualization of cerebral blood vessels have been introduced by [37]. The focus in this work is on shading techniques emphasizing the curvature of vessels as well as the efficient computation of the resulting surface-based visualizations.

VI. Conclusion

We have presented methods for the analysis and visualization of hepatic vasculature and for the approximation of vascular territories. Our analysis of eight human corrosion casts revealed the accuracy of the methods for the prediction of vascular territories. The approximation algorithms are also employed to suggest tumor resections with respect to certain safety margins. In cases, with several metastases or a tumor in a central location, these suggestions are helpful because it is not obvious whether the patient is resectable at all.

The HQVV method for the visualization of vasculature is inspired by the visualizations in traditional teaching materials. We have attempted to create 3-D visualizations of a similar quality with two additional advantages: the visualizations reveal patient-specific branching patterns and can be explored interactively.

The methods presented here are not bound to classical liver surgery planning, but may also be relevant for minimally invasive therapies for the ablation of liver tumors. Several organs within the human body, e.g., the lung, the kidney, and the pancreas, are also characterized by hierarchical vessel systems. We have applied our methods to lung segment approximation and have evaluated them by comparing the results utilizing *in vitro* specimens [20]. Vessel analysis techniques have also been applied to intracranial arteries and to quantify abdominal aortic stents [33].

Much effort was spent on the integration of the algorithms in a software assistant, called HepaVision. This software has been used at various hospitals to plan some 130 oncologic resections and 40 LRLTs so far.

Acknowledgment

The authors would like to thank their colleagues, C. Evertsz, H. Hahn, G. Prause, and W. Spindler. The Laplace approximation is inspired by C. Evertsz. W. Spindler developed the visualization tools used at MeVis and prepared some of the images used in this paper. The HQVV method was developed by H. Hahn. The authors also would like to thank all the members of the following institutions for their substantial support: the Department of Morphology, University Medical Center Geneva, Geneva, Switzerland (J. Fasel), the Department of Diagnostic Radiology, Medical School Hannover, Hannover, Germany (M. Galanski), the Department of Diagnostic Radiology, Philipps University Marburg, Marburg, Germany (K. J. Klose), and the Department of General and Transplantation Surgery, University Hospital Essen, Essen, Germany (K. J. Oldhafer).

References

[1] "Fractals in physics—Proc. Int. Conf. Honouring B. Mandelbrot," *Physica D*, vol. 38, no. 1–3, 1989.

[2] C. Barrilot, B. Gibaud, J. Scarabin, and Coatrieux, "3-D reconstruction of cerebral blood vessels," *IEEE Comput. Graph. Applicat.*, vol. CGA-5, pp. 13–19, 1985.

[3] H. A. Blum, *Transformation for Extracting New Descriptors of Shapes. Models for the Perception of Speech and Visual Form*, W. Wathen-Dunn, Ed. Cambridge, MA: MIT Press, 1967, pp. 362–380.

[4] C. C. Le Foie, *Etudes Anatomiques et Chirurgicales*. Paris, France: Masson, 1957.

[5] E. E. Danielsson, "Euclidean distance mapping," *Comput. Graph. Image Processing*, vol. 14, pp. 227–248, 1980.

[6] E. R. Davies and A. P. N. Plummer, "Thinning algorithms: A critique and a new methodology," *Pattern Recogn.*, vol. 14, no. 1, pp. 53–63, 1981.

[7] P. Dokladal, C. Lohou, L. Perroton, and G. Bertarnd, "Liver blood vessel extraction by a 3-D topological approach," in *Proc. Medical Image Computing and Computer-Assisted Intervention (MICCAI 1999)*, vol. 1679, Lecture Notes in Computer Science, pp. 98–105.

[8] C. J. G. Evertsz, "Laplacian fractals," Ph.D. dissertation, Univ. Groningen, Groningen, The Netherlands, 1989.

[9] C. J. G. Evertsz, H.-O. Peitgen, and R. F. Voss, Eds., *Fractal Geometry and Analysis. The Mandelbrot Festschrift*. Curaçao, The Netherlands: World Scientific, 1996.

[10] A. X. Falcao, K. Jayaram, J. K. Udupa, and F. K. Miyazawa, "An ultra-fast user-steered image segmentation paradigm: Live-wire-on-the-fly," in *Proc. SPIE Medical Imaging 1999*, vol. 3661, Newport Beach, CA, pp. 184–191.

[11] J. H. D. Fasel, D. Selle, P. Gailloud, C. J. G. Evertsz, F. Terrier, and H.-O. Peitgen *et al.*, "Segmental anatomy of the liver: Poor correlation with CT," *Radiol.*, vol. 206, no. 1, pp. 151–156, 1998.

[12] B. B. Frericks, F. C. Caldarone, A. Schenk, D. Selle, B. Preim, H.-O. Peitgen, M. Galanski, B. Nashan, and J. Klempnauer, "New computational methods for the evaluation of living related liver donation," presented at the Transplant 2001 Conf., Chicago, IL, May 2001.

[13] G. Gerig, T. Koller, G. Szkely, C. Brechbühler, and O. Kübler, "Symbolic description of 3-D structures applied to cerebral vessel tree obtained from MR angiography volume data," in *Information Processing in Medical Imaging*, 1993, vol. 687, Lecture Notes in Computer Science, pp. 94–111.

[14] G. Glombitza, W. Lamade, and A. M. Demiris, "Technical aspects of liver resection planning MedInfo '98," in *Proc. 9th World Congr. Medical Informatics*, 1998, pp. 1041–1045.

[15] G. Glombitza, W. Lamade, A. M. Demiris, and C. Herfarth *et al.*, "Virtual planning of liver resections: Image processing, visualization and volumetric evaluation," *Int. J. Med. Inform.*, vol. 53, no. 2–3, pp. 225–237, 1999.

[16] H. K. Hahn, C. J. G. Evertsz, J. H. D. Fasel, and H.-O. Peitgen, "Fractal properties, segment anatomy and interdependence of the human portal vein and the hepatic vein," *Fractals*, to be published.

[17] H. K. Hahn, B. Preim, D. Selle, and H.-O. Peitgen, "Visualization and interaction techniques for the exploration of vascular structures," in *Proc. Visualization 2001*, San Diego, CA, pp. 395–402.

[18] D. Högemann, G. Stamm, K. J. Oldhafer, D. Selle, T. Schindewolf, and M. Galanski, "Volumetric evaluation and 3-D visualization of the liver before living-related donation," in *Proc. Computer Assisted Radiology and Surgery (CARS 1999)*, Paris, France, pp. 249–252.

[19] T. Y. Kong and A. Rosenfeld, "Digital topology: Introduction and survey," *Comput. Vis. Graph. Image Processing*, vol. 48, pp. 357–397, 1989.

[20] S. Krass, D. Selle, D. Böhm, H. Jend, A. Kriete, W. Rau, and H.-O. Peitgen, "Determination of bronchopulmonary segments based on HRCT data," in *Proc. Computer Assisted Radiology and Surgery (CARS 2000)*, San Francisco, CA, pp. 584–589.

[21] L. Lam, S. W. Lee, and C. Y. Suen, "Thinning methodologies—A comprehensive survey," *IEEE Trans. Pattern Anal. Machine Intell.*, vol. 14, pp. 869–885, Sept. 1992.

[22] W. Lamade, G. Glombitza, L. Fischer, P. Chiu, C. E. Cardenas, and M. Thorn *et al.*, "The impact of 3-dimensional reconstructions on operation planning in liver surgery," *Arch. Surgery*, vol. 135, no. 11, pp. 1256–1261, 2000.

[23] T.-C. Lee, R. L. Kashyap, and C. N. Chu, "Building skeleton models via 3-D medial surface/axis thinning algorithms," *Graph. Models Image Processing*, vol. 56, no. 6, pp. 462–478, 1994.

[24] T. Lei, J. K. Udupa, P. K. Saha, and D. Odhner, "Separation of artery and vein in contrast enhanced MRA images," in *Proc. SPIE Medical Imaging 2000*, vol. 978, San Diego, CA, pp. 233–244.

[25] T. Lei, J. K. Udupa, and P. K. Saha, "Artery–vein separation via MRA—An image processing approach," *IEEE Trans. Med. Imag.*, vol. 20, pp. 689–703, Aug. 2001.

[26] C. Lorenz, I. C. Carlssen, T. M. Buzug, C. Fassnacht, and J. Weese, "Multi-scale line segmentation with automatic estimation of width, contrast, and tangential direction in 2-D/3-D medical images," in *Proc. CVRMed/MRCAS 1997*, vol. 1205, Lecture Notes in Computer Science, pp. 233–242.

[27] B. Mandelbrot, *Die Fraktale Geometrie der Natur*. Basel, Switzerland: Birkhäuser, 1987.

[28] M. E. Martinez-Perez, A. D. Hughes, A. V. Stanton, S. A. Thom, A. A. Bharath, and K. H. Parker, "Retinal blood vessel segmentation by means of scale-space analysis and region-growing, medical image computing and computer-assisted intervention," in *Proc. MICCAI 1999*, vol. 1679, Lecture Notes in Computer Science, Cambridge, MA, pp. 90–97.

[29] Y. Masutani, K. Masamune, and T. Dohi, "Region-growing-based feature extraction algorithm for tree-like objects, visualization in biomedical computing," in *Proc. VBC 1996*, vol. 1131, Lecture Notes in Computer Science, Hamburg, Germany, pp. 161–171.

[30] E. N. Mortensen, B. S. Morse, W. A. Barrett, and J. K. Udupa, "Adaptive boundary detection using live-wire two-dimensional dynamic programming," in *Proc. Computers in Cardiology*, Durham, NC, Oct. 1992, pp. 635–638.

[31] F. H. Netter, *Atlas of the Human Anatomy*, 8th ed. Summit, NJ: Ciba Geigy, 1995.

[32] H. J. Noordmanns and A. W. M. Smeulders, "High accuracy tracking of 2-D/3-D curved line structures by consecutive cross section matching," *Pattern Recogn. Lett.*, vol. 19, no. 5, pp. 97–111, 1998.

[33] G. Prause, D. Selle, and H.-O. Peitgen, "Morphometric and structural analysis of vasculature in volumetric images," in *Proc. Computer Assisted Radiology and Surgery (CARS 2001)*, vol. ICS 1230, Berlin, Germany, pp. 947–951.

[34] B. Preim, D. Selle, W. Spindler, K. J. Oldhafer, and H.-O. Peitgen, "Interaction techniques and vessel analysis for preoperative planning in liver surgery medical image computing and computer-assisted intervention," in *Proc. MICCAI 2000*, Lecture Notes in Computer Science, Pittsburgh, PA, 1935, pp. 608–617.

[35] B. Preim, D. Selle, W. Spindler, and H.-O. Peitgen, "3-D interaction techniques for planning oncologic soft tissue operations," in *Proc. Graphics Interface*, Ottawa, ON, Canada, June 2001, pp. 183–190.

[36] W. H. Press, S. A. Teukolsky, W. T. Vetterling, and B. P. Flannery, *Numerical Recipes in C*. Cambridge, U.K.: Cambridge Univ. Press, 1993.

[37] A. Puig, D. Tost, and I. Navazo, "An interactive cerebral blood vessel exploration system," in *Proc. Visualization 1997*, Phoenix, AZ, pp. 433–436.

[38] S. P. Raya and J. K. Udupa, "Shape-based interpolation of multidimensional objects," *IEEE Trans. Med. Imag.*, vol. 9, pp. 32–42, Feb. 1990.

[39] B. L. Rice and J. K. Udupa, "Fuzzy-connected clutter-free volume rendering for MRA," *Int. J. Imag. Syst. Technol.*, vol. 11, pp. 62–70, 2000.

[40] A. Schenk, G. Prause, and H.-O. Peitgen, "Efficient semiautomatic segmentation of 3-D objects in medical images ," in *Proc. MICCAI 2000*, vol. 1935, Lecture Notes in Computer Science, pp. 186–195.

[41] ——, "Local cost computation for efficient segmentation of 3-D objects with live wire," in *Proc. SPIE Medical Imaging 2001: Image Processing*, vol. 4322, San Diego, CA, pp. 1357–1364.

[42] D. Selle, "Analysis of vessel structures in medical volume data for the computer-aided planning of surgical interventions," Ph.D. dissertation, Univ. Bremen, Bremen, Germany, 2000. In German.

[43] D. Selle, W. Spindler, B. Preim, and H.-O. Peitgen, "Mathematical methods in medical imaging: Analysis of vascular structures for liver surgery planning," in *Mathematics Unlimited*, B. Engquist and W. Schmid, Eds. Berlin, Germany: Springer-Verlag, 2001, pp. 1039–1059.

[44] D. Selle and H.-O. Peitgen, "Analysis of the morphology and structure of vessel systems using skeletonization," in *Proc. SPIE Medical Imaging 2001*, vol. 4321, pp. 271–281.

[45] L. Soler, H. Delingette, and G. Malandain *et al.*, "Fully automatic anatomical, pathological and functional segmentation from CT scans for hepatic surgery," in *Proc. SPIE Medical Imaging 2000*, vol. 3979, pp. 246–255.

[46] L. Soler, H. Delingette, and G. Malandain *et al.*, "Fully automatic anatomical, pathological and functional segmentation from CT scans for hepatic surgery," *Comput. Aided Surg.*, vol. 6, no. 3, pp. 131–142, Aug. 2001.

[47] M. Sonka, A. Stolpen, W. Liang, and R. M. Stefancik, *Vascular Imaging and Analysis. Handbook of Medical Imaging, Vol. 2, Medical Image Processing and Analysis*, M. Sonka and J. M. Fitzpatrick, Eds. Bellingham, WA: SPIE Press, 2001, pp. 809–914.

[48] M. Sonka, R. M. Stefancik, and S. Tadikonda, "Feasibility of automated separation of arteries and veins in contrast-enhanced MRA using a graph searching technique," in *Proc. 3rd Annu. Meeting Int. Soc. Magnetic Resonance in Medicine (ISMRM)*, 1999, p. 2183.

[49] J. K. Udupa, S. Samarasekera, and W. A. Barrett, "Boundary detection via dynamic programming," in *Proc. Visualization in Biomedical Computing*, Chapel Hill, NC, 1992, pp. 33–39.

[50] J. K. Udupa, L. Wei, S. Samarasekera, Y. Miki, M. A. van Buchem, and R. I. Grossman, "Multiple sclerosis lesion quantification using fuzzy-connectedness principles," *IEEE Trans. Med. Imag.*, vol. 16, pp. 598–609, Oct. 1997.

[51] O. Wink, W. Niessen, and M. Viergever, "Fast quantification of abdominal aortic aneurysms from CTA volumes," in *Proc. Medical Image Computing and Computer-Assisted Intervention (MICCAI 1998)*, vol. 1432, Lecture Notes in Computer Science, pp. 138–145.

[52] ——, "Fast delineation and visualization of vessels in 3-D angiographics images," *IEEE Trans. Med. Imag.*, vol. 19, pp. 337–346, Apr. 2000.

[53] P. J. Yim, P. L. Choyke, and R. M. Summers, "Greyscale skeletonization of small vessels in MRA," *IEEE Trans. Med. Imag.*, vol. 19, pp. 568–576, June 2000.

[54] P. J. Yim, R. Mullick, R. M. Summers, Marcos, J. A. Cebral, R. Lohner, and P. L. Choyke, "Measurement of stenosis from magnetic resonance angiography using vessel skeleton," in *Proc. SPIE Medical Imaging 2000* , vol. 3978, San Diego, CA, 2000, pp. 245–255.

[55] P. J. Yim, P. L. Choyke, and R. M. Summers, "Locating bloodvessels in retinal images by piecewise threshold probing of a matched filter response," *IEEE Trans. Med. Imag.*, vol. 19, pp. 203–210, Mar. 2000.